Numerical modeling of the cupular displacement and motion of otoconia particles in a semicircular canal

Tijana Djukic & Nenad Filipovic

Biomechanics and Modeling in Mechanobiology

ISSN 1617-7959

Biomech Model Mechanobiol
DOI 10.1007/s10237-017-0912-8

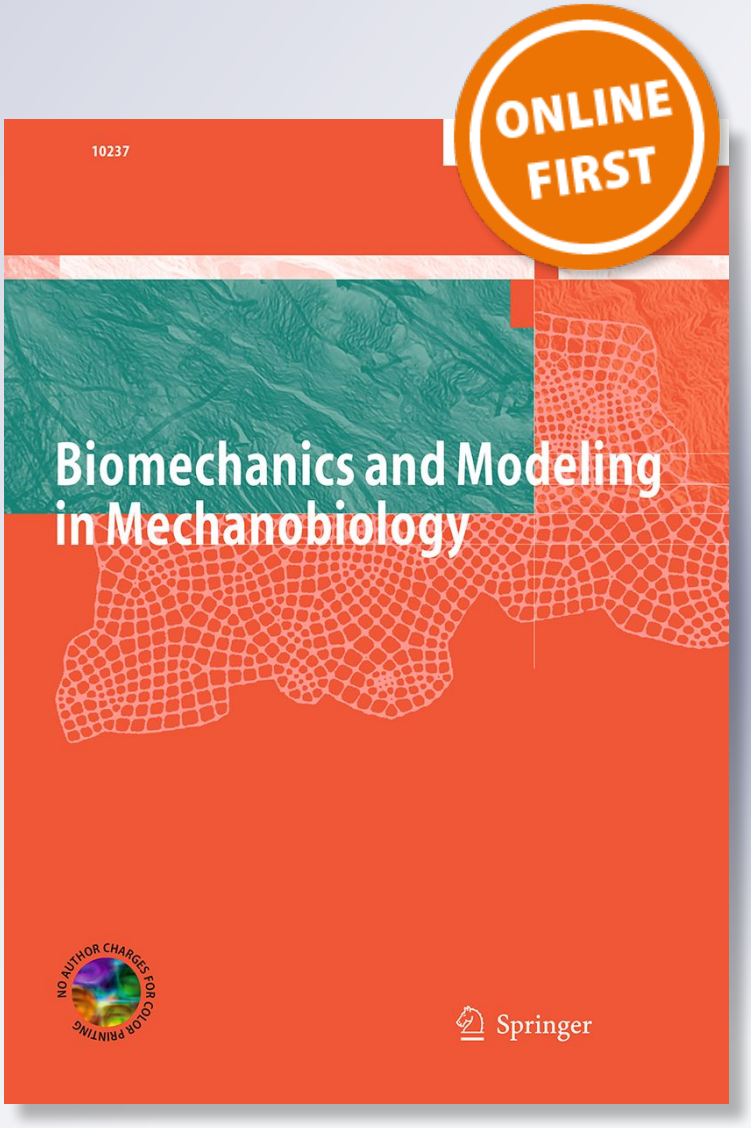

Springer

Biomech Model Mechanobiol
DOI 10.1007/s10237-017-0912-8

ORIGINAL PAPER

Numerical modeling of the cupular displacement and motion of otoconia particles in a semicircular canal

Tijana Djukic[1,2] · **Nenad Filipovic**[1,2]

Received: 2 July 2016 / Accepted: 21 April 2017

Abstract Balance is achieved and maintained by a balance system called a labyrinth that is composed of three semicircular canals and the otolith organs that sense linear gravity and acceleration. Within each semicircular canal, there is a gelatinous structure called the cupula, which is deformed under the influence of the surrounding endolymph. One of the balance disorders is benign paroxysmal positional vertigo, and one of the pathological conditions that have been identified as possible causes of this syndrome is canalithiasis—disturbance of the endolymph flow and cupular displacement caused by the free-moving otoconia particles within the lumen of the canal. Analysis of phenomena occurring within the semicircular canal can help to explain some balance-related disorders and the response of the vestibular system to external perturbations under various pathological conditions. Numerical simulations allow a study of the influence of a wide range of factors, without the need to perform experiments and clinical examinations. In case of canalithiasis, an accurate explanation and tracking of the motion of otoconia particles in vivo is obviously nearly impossible. In this study, a numerical model was developed to predict the motion of otoconia particles within the semicircular canal and the effect of the endolymph flow and particles on the deformation of the cupula.

✉ Tijana Djukic
tijana@kg.ac.rs

Nenad Filipovic
fica@kg.ac.rs

[1] R&D Center for Bioengineering, BioIRC, Prvoslava Stojanovica 6, Kragujevac 34000, Serbia

[2] Faculty of Engineering, University of Kragujevac, Kragujevac, Serbia

Keywords Balance · Vestibular system · Endolymph flow · Deformable membrane · Immersed particles · Solid–fluid interaction

1 Introduction

Balance is the ability to maintain the body in the appropriate position while standing or walking. A properly functioning balance system allows humans to identify its orientation, see clearly during motion, determine direction, speed of movement and overall spatial awareness. Balance is achieved and maintained by a complex set of sensorimotor control systems. One of the organs that is part of the balance system is called a labyrinth and it is located within the inner ear. This organ is composed of three semicircular canals (SCCs) that are mutually orthogonal. Each SCC is filled with fluid called endolymph that has characteristics similar to water. When the head is moved, the fluid within the SCC also moves. On one end of the SCC, there is a widened region, called ampulla, within which there is a gelatinous structure called the cupula. The cupula covers the entire cross section of the SCC and it contains sensory hair cell receptors. The human vestibular system is illustrated in Fig. 1. The fluid flow within the SCC causes a deformation of the cupula. Due to this deformation, the sensory hair cells register the movement, and ultimately, nerve signals are sent to the brain, to inform it in which direction the head just turned. These information lead to an eye movement that should compensate for the head movement and ensure that the focus of the eyes is conserved. The eye movement can be quantified by a velocity called nystagmus velocity. In this study, it is assumed that the nystagmus velocity is proportional to the displacement of the cupula, according to the previous analysis presented in the literature (Obrist and Hegemann 2008; Squires et al. 2004).

Published online: 03 May 2017

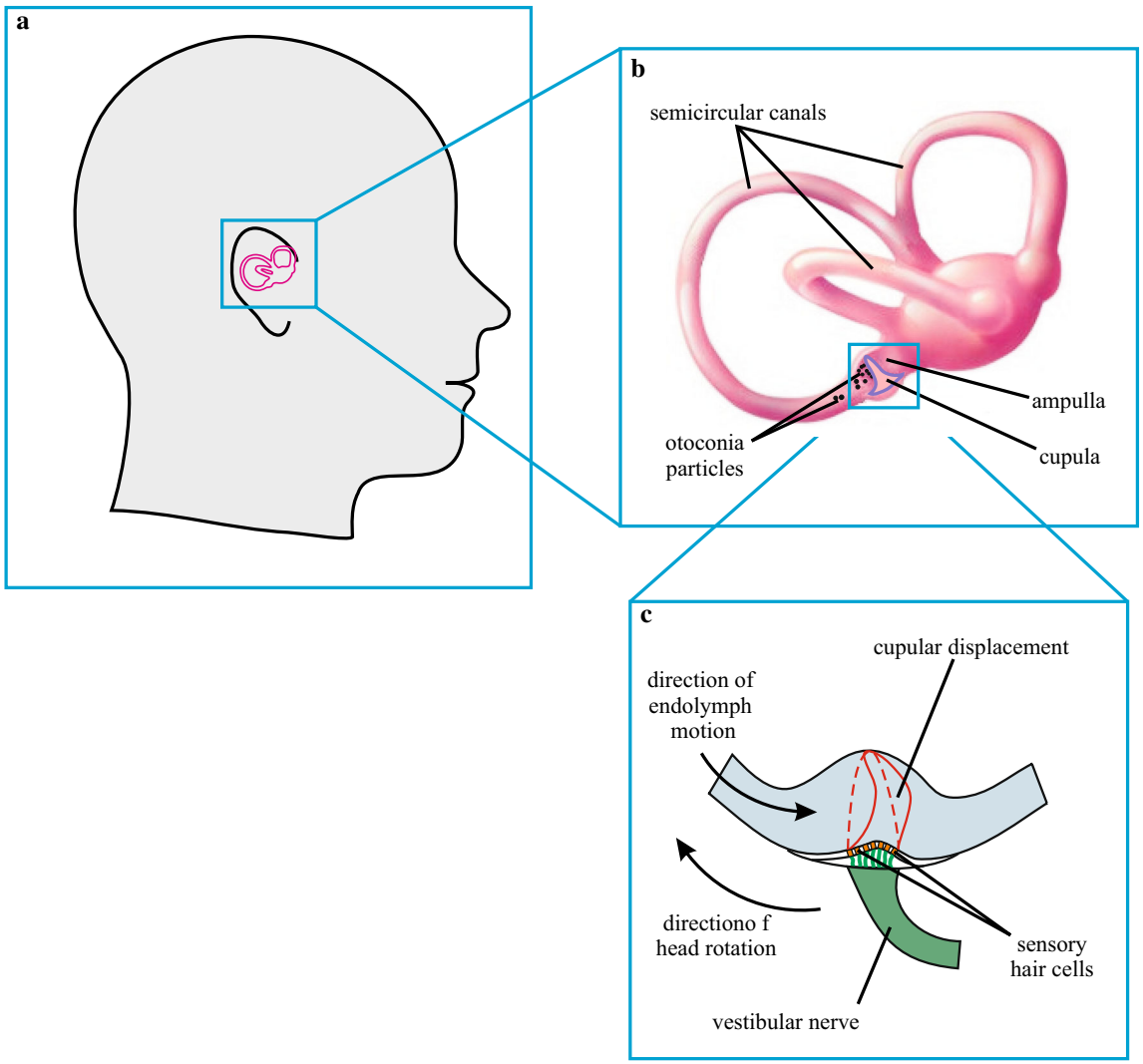

Fig. 1 Human vestibular system. **a** Position of the SCCs in the human head; **b** Position of the cupula within the SCC; **c** Cupular deformation during the rotation of the head

The causes of balance disorders can be multiple, such as neurological, medical (for example, high blood pressure), psychological (for example, anxiety) and pathologies of the inner ear. In 20–30% of balance disorders, the syndrome is called benign paroxysmal positional vertigo (BPPV) (Baloh et al. 1989). Patients suffering from BPPV experience symptoms such as imbalance, impaired vision and dizziness. There are two pathological conditions that have been identified as possible causes of BPPV: cupulolithiasis (Schuknecht 1962) and canalithiasis (Brandt and Steddin 1993; Hall et al. 1979).

Besides the SCCs, there is another vestibular organ called the otolith organ. It contains crystals of calcium carbonate. These calcite particles (otoconia) are constantly shed, dissolved and replaced by new ones. But, in some cases, these particles do not dissolve fast enough or there are too many particles, so they enter the SCC and affect the flow of endolymph and subsequently the displacement of the cupula. This disturbance caused by the free-moving trapped particles within the lumen of the SCC causes canalithiasis and positional nystagmus. The presence of mentioned particles in the SCC has been clinically observed in patients suffering from BPPV (Parnes and McClure 1992).

The analysis of phenomena occurring within the SCC can help to explain some balance-related disorders and the response of the vestibular system to external perturbations under various pathological conditions. Numerical simulations can be a useful tool in this analysis, because they allow a study of the influence of a wide range of factors, without the need to perform experiments and clinical examinations. In case of canalithiasis, an accurate explanation and tracking of the motion of otoconia particles in vivo is obviously nearly impossible. However, using some approximations and known facts about the vestibular system, it is possible to create a numerical model that can help to understand this syndrome.

House and Honrubia (2003) analyzed the BPPV disorder and created physicomathematical models to describe the phenomena occurring within the SCC, such as cupulolithiasis and canalithiasis. Rajguru and Rabbitt (2007) have analyzed the information about angular velocity that were sent to the brain during the induced canalithiasis. Their experiments were performed in vivo in an animal model. Other authors have also analyzed the canalithiasis experimentally in animal models (Inagaki et al. 2006; Suzuki et al. 1996). All these studies confirmed that the movement of otoconia particles within the lumen of the SCC can cause symptoms that are connected with BPPV. In this study, a numerical model was developed to predict the motion of particles within the SCC and the effect of the fluid flow and particles on the deformation of the cupula. Variation in some of the parameters of the model was performed, and the effect of this change on the cupular displacement was also analyzed. This model could help to predict the response of the vestibular system of the clinical patient during head maneuvers, and it can help early diagnostics, treatment planning, and tracking of the progress of the balance disorder.

The paper is organized as follows. In Sect. 2, the proposed numerical model was explained in detail. Section 3 defines the parameters of the model and lists other relevant information needed to perform the simulations. Results of the numerical simulations are presented in Sect. 4. Section 5 discusses other theoretical and numerical models presented in literature, lists conclusions drawn from the presented study and suggests further improvements that will be conducted.

2 Materials and methods

2.1 Modelling fluid flow with moving boundaries

Fluid flow with moving boundaries is modeled using the mass-conserved volumetric lattice Boltzmann (abbreviated MCVLB) method (Yu et al. 2014). This is a special adaptation of the basic lattice Boltzmann (LB) method (Malaspinas 2009; Djukic 2015). Due to its characteristics, the implementation of this method is relatively simple and parallelization techniques can be applied to speed up the calculations. LB method was successfully applied to model the motion of LDL (low-density lipoprotein) particles through the bloodstream (Filipovic et al. 2014), to analyze and predict the motion of nanodrugs through the bloodstream (Filipovic et al. 2012) and circulating cancer cells through microfluidic chip (Djukic et al. 2015). In all mentioned cases, the blood flow is modeled as the flow of a Newtonian fluid, with immersed deformable or non-deformable particles, that affect the fluid flow. Another advantage of the LB method is the fact that it can successfully simulate fluid flow on a large scale of Reynolds number—from the values of less than 1, like it is the case in blood flow through the capillary network (Sun and Munn 2008), to very large numbers, like it is the case in the blood flow through the human aorta (Krafczyka et al. 1998). This method can be successfully applied to model the endolymph flow in the SCC. This was demonstrated through a good agreement of results that was obtained when results of the proposed numerical model were compared with results from the literature where traditional methods of computational fluid dynamics were applied. These comparisons are presented in Sect. 4.

In the standard LB method, fluid particles are fixed to a Cartesian mesh. A special propagation function is defined, and this function depends on the state of neighboring particles and has an identical form for all the particles, i.e., for all the nodes in the lattice mesh. Motion of fluid particles is studied through their mutual collisions at lattice nodes and further propagation in the observed domain in the prescribed directions. It can be demonstrated that the fluid flow can be modeled at the macroscale level by modeling the fluid at a microscale level and by tracking the dynamics of discrete particles. It is necessary to perform a certain derivation procedure in order to transform the basic equations of the LB method to a system of equations that is used in fluid dynamics—continuity equation and Navier–Stokes equation. There are several approaches to obtain the required equations, one of them was first applied by Huang (1987) and it is also explained in the literature (Malaspinas 2009; Djukic 2015). This derivation procedure proves that mass and momentum conservation laws are satisfied within the LB method.

The boundary condition (BC) used for fixed walls is called bounce-back BC. In the implementation of this BC, certain nodes of the mesh are denoted as solid nodes, i.e., as an obstacle. In all such nodes, the components of the distribution function are not evaluated in the same way as in the rest of the nodes. The components going from the fluid toward the boundary are reverted back to the fluid domain. Using this approach, the non-slip boundary condition is imposed. If the solid–fluid boundary is made of straight lines, then it is desirable to use this approach. But if complex geometries with curved boundaries are considered and/or the boundary is not fixed, then a more recent approach for simulating moving boundaries should be applied. This kind of motion is considered in this study, and hence, the adapted MCVLB method is used.

The adapted MCVLB method is developed for simulation of willfully moving arbitrary boundaries (Yu et al. 2014), where "willfully moving" means that the velocity of the boundary is predefined. In the implementation of this method, there are three steps. First, the collision of the particles is modeled, with special attention dedicated to the collisions of fluid particles with moving solid boundary. The second step is the streaming (propagation), which is performed such that a special type of bounce-back is applied to ensure the

interaction between fluid and solid. The third step is used to ensure mass conservation of fluid during the motion of solid boundary. The third step is not considered in this study, because in this case the boundary is not deformable and it moves along with the fluid in space, so there is no motion of the boundary with respect to the fixed Cartesian mesh.

In order to define the equations that are used in MCVLB method, first it is necessary to define two quantities fluid volume portion and particle distribution function. In the entire domain that is simulated, cells in the lattice mesh can be either occupied completely by solid, by fluid or partially by fluid and solid. Thus, cells have to be categorized based on the occupation of solid volume that is defined as:

$$P(\mathbf{x}, t) = \frac{\Delta V_s(\mathbf{x}, t)}{\Delta V} \tag{1}$$

where $\Delta V_s(\mathbf{x}, t)$ is the volume that solid occupies within the observed cell and ΔV is the overall cell volume, which is taken to be unity. If a cell is entirely occupied by fluid, then $P = 0$; if a cell is entirely occupied by solid, then $P = 1$, while $0 < P < 1$ if a cell is partially occupied by solid and partially by fluid.

The fluid volume portion is therefore given by:

$$\Delta V_f(\mathbf{x}, t) = [1 - P(\mathbf{x}, t)]\Delta V \tag{2}$$

The distribution function in standard LB method is denoted by f_i, while in MCVLB method, the distribution function is denoted by n_i. The relation between these two quantities is defined using the following equation:

$$f_i(\mathbf{x}, t) = n_i(\mathbf{x}, t)/\Delta V_f(\mathbf{x}, t) \tag{3}$$

The collision of the particles is modeled using the following equation:

$$n_i'(\mathbf{x}, t) = n_i(\mathbf{x}, t) - \frac{1}{\tau}\left(n_i(\mathbf{x}, t) - n_i^{(0)}(\mathbf{x}, t)\right) + \left(1 - \frac{1}{2\tau}\right)\mathbf{F}_i \tag{4}$$

where the superscript $'$ denotes the values of distribution function after collision, τ represents the relaxation time, $\mathbf{F}_i$ represents the external force term and $n_i^{(0)}$ represents the equilibrium particle distribution function, which is calculated as:

$$n_i^{(0)}(\mathbf{x}, t)) = N\omega_i\left[1 + \frac{\xi_i \cdot \mathbf{U}}{c_s^2} + \frac{(\xi_i \cdot \mathbf{U})^2}{2c_s^4} - \frac{\mathbf{U} \cdot \mathbf{U}}{2c_s^2}\right] \tag{5}$$

where $N(\mathbf{x}, t) = \Sigma n_i(\mathbf{x}, i)$, c_s represents the constant related to the LB method, defined by $c_s^2 = \frac{1}{3}$ and ξ_i represent vectors defining the abscissae of the lattice structure. In this study, the three-dimensional isothermal flow of incompressible fluid is simulated and the lattice structure denoted by D3Q27 is used.

The external force term $\mathbf{F}_i$ is defined in terms of the external force field acting on the fluid $\mathbf{g}$:

$$\mathbf{F}_i = \omega_i\left[\frac{\xi_i - \mathbf{U}}{c_s^2} + \frac{(\xi_i \cdot \mathbf{U})\xi_i}{c_s^4}\right]\mathbf{g}(\mathbf{x}, t) \tag{6}$$

Equation (5) which is used in MCVLB method differs from the equation for equilibrium particle distribution function in standard LB method only in the value of velocity $\mathbf{U}$. Instead of macroscopic velocity $\mathbf{u}$ that is used in standard LB method, the velocity in this case is defined such that $\mathbf{U} = \mathbf{u} + \delta\mathbf{u}$, in order to take into account the effect of moving boundary, where $\delta\mathbf{u}$ is defined as follows:

$$\delta\mathbf{u} = \tau P(\mathbf{x}, t)\mathbf{u}_B(\mathbf{x}, t) + \frac{\tau \sum_j P(\mathbf{x} + \xi_j, t)n_j(\mathbf{x}, t)\mathbf{u}_B(\mathbf{x} + \xi_j, t)}{N(\mathbf{x}, t)} \tag{7}$$

where $\mathbf{u}_B(\mathbf{x}, t)$ is the velocity of the boundary in considered lattice cell at considered time point.

The propagation of particles is modeled using the following equation:

$$n_i''(\mathbf{x}, t) = [1 - P(\mathbf{x}, t)]n_i'(\mathbf{x} - \xi_i\Delta t, t) + P(\mathbf{x} + \xi_{i*}\Delta t, t)n_{i*}^{'}(\mathbf{x}, t) \tag{8}$$

where the index $i*$ corresponds to the direction opposite to the ith direction, i.e., $\xi_{i*} = -\xi_i$. Equation (8) ensures that mass is conserved over the whole domain. When this equation is applied to a cell entirely occupied by fluid (when $P = 0$), Eq. (8) is identical to the equation used for propagation in standard LB method.

Macroscopic quantities, such as pressure and velocity, can be calculated using the components of the particle distribution function.

Pressure is calculated as:

$$p = c_s^2\frac{\sum_i n_i(\mathbf{x}, i)}{1 - P(\mathbf{x}, t)} \tag{9}$$

The expression for physical velocity is given by:

$$\mathbf{u} = \frac{\xi_i \sum_i n_i(\mathbf{x}, i)}{\sum_i n_i(\mathbf{x}, i)} + \frac{\mathbf{g}}{2} \tag{10}$$

2.2 Modeling solid–fluid interaction

The modeling of solid–fluid interaction was employed both for the cupula and the immersed particle, but in slightly modified way. The immersed boundary method (IBM) that was first presented by Peskin (Peskin 1977) was used in this study.

In IBM, fluid domain is represented with a fixed Cartesian mesh; immersed objects are treated as a separated part of the fluid; and the boundary between two domains is represented with a set of Lagrangian points. This boundary is assumed to be easily deformable, with high stiffness (Wu and Shu 2010). All entities (endolymph, cupula and particle) are modeled simultaneously, as if it was a single mechanical system. The cupula and particle are affecting the surrounding fluid, and this is modeled using an external force field that is introduced in the equations for modeling the fluid flow. On the other hand, the fluid is causing the deformation of the cupula through a force that deforms the boundary between two domains and also the fluid is opposing the motion of the particle through a drag force.

In numerical simulations, meshes of different densities are used for discretization of the fluid domain and the cupula, and hence, the coupling is performed such that all relevant quantities are calculated using interpolation over the boundary points. For each node of the mesh representing the cupula, the influence of a larger number of points from the fixed fluid mesh is considered and vice versa.

Dirac delta function is used for interpolation of quantities, and this function is defined as:

$$\delta\left(\mathbf{x}-\mathbf{X}_B(t)\right)=D_{ijk}\left(\mathbf{x}_{ijk}-\mathbf{X}_B^l\right)= =\delta\left(x_{ijk}-X_B^l\right)\delta\left(y_{ijk}-Y_B^l\right)\delta\left(z_{ijk}-Z_B^l\right) \tag{11}$$

where the coordinates of lth node are denoted by $\mathbf{X}_B^l(t)$, $l=1,2,\ldots,L$, L is the number of nodes in the mesh representing the membrane, and indexes i, j and k denote the currently considered point in the fluid mesh.

The value of function $\delta(r)$ is defined in the literature (Peskin 1977):

$$\delta(r)=\begin{cases}\frac{1}{4h}\left(1+cosd\left(\frac{\pi}{r}2\right)\right) & |r|\le 2\\ 0 & |r|>2\end{cases} \tag{12}$$

where h denotes the distance between two points of the fluid mesh (in this study, since LB method is considered, $h=1$).

Applying this interpolation scheme, the external force field that is introduced in fluid flow equations can be defined as:

$$\mathbf{g}(\mathbf{x}_{ijk},t)=\sum_{l=1}^{L}\mathbf{F}_l(t)D_{ijk}\left(\mathbf{x}_{ijk}-\mathbf{X}_B^l(t)\right) \tag{13}$$

where $\mathbf{F}(t)$ is the force with which the cupula opposes the effect of the fluid, which is calculated as described in Sect. 2.3.

The nodes of the mesh representing the cupula are moved due to the effect of the surrounding fluid. First, the velocity of the nodes can be calculated using interpolation over the surrounding points in fluid mesh, using the following equation:

$$\mathbf{u}_B^l=\sum_{i,j,k}\mathbf{u}\left(\mathbf{x}_{ijk},t\right)D_{ijk}\left(\mathbf{x}_{ijk}-\mathbf{X}_B^l\right) \tag{14}$$

Then, the new position of the nodes can be calculated, applying the Euler Forward method on Eq. (14):

$${}^{t+\Delta t}\mathbf{X}_B^l={}^{t}\mathbf{X}_B^l+\mathbf{u}_B^l\Delta t \tag{15}$$

The new positions of nodes have, of course, caused a deformation of the cupula. This deformation causes a reaction force that is opposing this deformation. The calculation of this force is explained in Sect. 2.3. This reaction force is reintroduced into the fluid flow equations using the already defined external force field. The described process is performed in iterations, which ensures that all domains are modeled simultaneously.

2.3 Modeling deformation of the cupula

In this study, it is considered that the cupula has negligible thickness and it is made of a certain number of points that are interconnected. This is the representation that is used by most models presented in the literature, e.g., by Obrist and Hegemann (2008). Therefore, the discretization is performed such that the cupula is divided on a defined number of triangles. In a mesh that is created this way, it is possible to determine the reaction force for every element and for every node of the mesh. This reaction force represents the resistance of a particular node to the defined external deformation. In this study, the cupula is treated as a set of nodes that are interconnected with springs, i.e., as a linearly elastic material. This approach was proposed by Dupin et al. (2007). In this case, every movement of the nodes causes a spring force that can be defined as:

$$\mathbf{F}_{j_1}^{\mathrm{S}}=-\mathbf{F}_{j_2}^{\mathrm{S}}=K^{\mathrm{S}}\frac{L_{12}-{}^{0}L_{12}}{{}^{0}L_{12}}\mathbf{l}_{12} \tag{16}$$

where K^{S} represents the parameter of resistance to surface strain, i.e., the cupular stiffness [the value is defined according to the values used in the literature (Obrist and Hegemann 2008)], L_{12} and ${}^{0}L_{12}$ denote the current distance between nodes j_1 and j_2 and the initial distance between considered nodes, respectively, and $\mathbf{l}_{12}$ denotes the unit vector that connects nodes j_1 and j_2.

2.4 Modeling motion of the particle

Particle is considered to be a rigid body that can move freely through the fluid, has mass m_p, density ρ_p and radius a_p.

There are several forces that influence the motion of the particle: gravitational force $\mathbf{F}_g$, Stokes drag force that represents the influence of the surrounding fluid $\mathbf{F}_S$ and inertial forces that are caused by the angular motion of the entire domain. The position vector of the particle $\mathbf{x}_p$ in each iteration is calculated using the following equation of motion:

$$m_p\left(\ddot{\mathbf{x}}_p + x_R\ddot{\alpha}\right) = \mathbf{F}_S + \mathbf{F}_g + \mathbf{F}_C \tag{17}$$

where x_R represents the distance of the particle from the center of rotation of the entire domain, $\ddot{\alpha}$ is the angular acceleration of the entire domain and $\mathbf{F}_C$ is the inertial force caused by the motion of the entire domain.

The forces in Eq. (17) are calculated as follows:

$$\mathbf{F}_S = -6\pi\nu\rho a_p\left(\dot{\mathbf{x}}_p - \mathbf{u}_p\right) \tag{18}$$

$$\mathbf{F}_g = -m_p\left(1 - \frac{\rho}{\rho_p}\right)\mathbf{G} \tag{19}$$

$$\mathbf{F}_C = m_p\left(\dot{\alpha}\times\dot{\alpha}\times\mathbf{x}_R + 2\dot{\alpha}\times\dot{\mathbf{x}}_p\right) \tag{20}$$

where $\mathbf{G}$ represents the gravity acceleration, $\dot{\alpha}$ is the angular velocity of the entire domain, ρ is fluid density, ν is fluid viscosity and $\mathbf{u}_p$ represents the fluid velocity in the particular point of the domain, i.e., at the current location of the particle $\mathbf{x}_p$.

When the particle during its motion comes close to the wall, i.e., when the distance between the particle and the closest wall is smaller than the predefined value of the lubrication gap χ, then an additional repulsive force normal to the wall is included in Eq. (17), to simulate the interaction between the particle and the wall of the SCC.

3 Simulation setup

The geometry of the SCC is simplified and it is assumed that the entire domain has a circular cross section, like it is shown in Fig. 2. Cupula is represented as a circle, with negligible thickness. The initial positions of both the cupula and the particle in numerical simulations are also shown in Fig. 2. Particle is assumed to be circular and its radius was varied, in order to analyze the effect of this change on the cupular displacement. Three different radii were considered in numerical simulations—15, 20 and 25 μm.

Material and geometrical parameters are taken from the literature (Obrist and Hegemann 2008; Squires et al. 2004; Van Buskirk et al. 1976) and are listed in Table 1.

During the initialization of the numerical simulation, the voxelization of the defined domain is performed to determine the occupation of solid volume in all nodes of the LB mesh. Voxelization is performed using the procedure described in the literature (Nooruddin and Turk 2003), and an additional open-source software Binvox, developed by

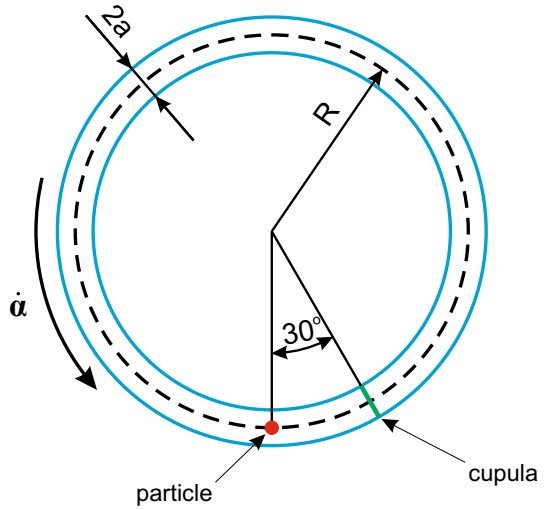

Fig. 2 Geometry of the simplified semicircular canal in numerical simulations

Table 1 Material and geometrical parameters (Obrist and Hegemann 2008; Squires et al. 2004; Van Buskirk et al. 1976)

Parameter	Value
Major canal radius, R	3.2×10^{-3} m
Duct radius, a	1.6×10^{-4} m
Endolymph density, ρ	10^3 kg m^{-3}
Endolymph viscosity, ν	10^{-6} m^2 s^{-1}
Particle density, ρ_p	2.7×10^3 kg m^{-3}
Lubrication gap, χ	1 μm

Patrick Min (Min 2013), is incorporated into the software. The voxelized model is further expanded to calculate the value of P for all nodes. The overall number of nodes in the created lattice mesh is around 250,000.

In all numerical simulations, the entire domain is rotated for 120°, to simulate a smooth head rotation from an upright position (when it is assumed that the degree of the head with respect to the vertical axis is 0°) to a supine position (when it is assumed that the degree of the head with respect to the vertical axis is 120°). This type of head rotation is used in diagnostics and clinical experiments of vestibular disorders and is known as the Dix–Hallpike maneuver (Dix and Hallpike 1952). Figure 3 shows the change of angle (left graph) and angular velocity (right graph) over time in all simulations.

During the implementation of the presented numerical model, parallelization techniques (principles of GPU (graphics processing units) programming and CUDA architecture developed by NVIDIA) were applied to ensure faster program execution. The computer program was developed such that compute-intensive parts of the program are executed on the GPU device, i.e., on the graphics card of the computer.

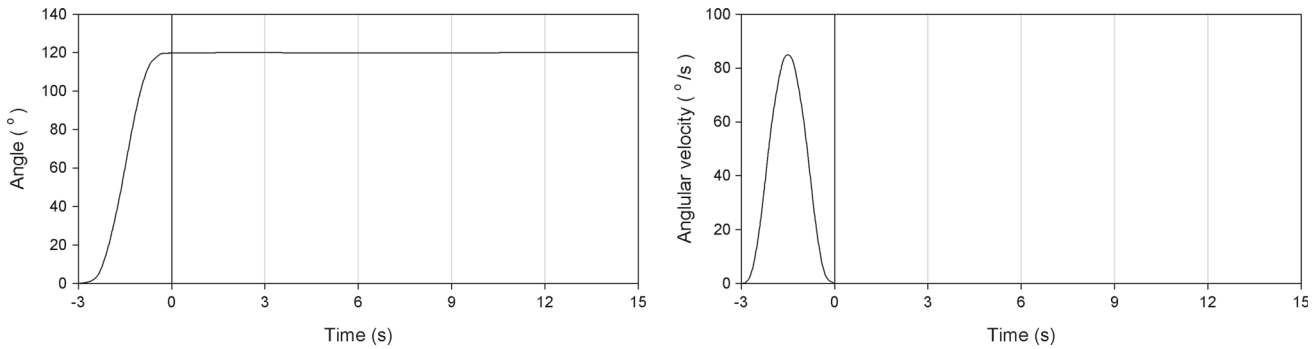

Fig. 3 Change of angle (*left*) and angular velocity (*right*) of the entire domain over time in numerical simulations

This practically means that instead of sequentially processing data about all lattice nodes and nodes representing the cupula, this data is processed in parallel and this ensures faster execution of the simulation. Using this approach, the execution time required for a single simulation is around 2–3 min.

4 Results

Results of simulations using the described numerical model were compared with analytical solutions presented in the literature (Obrist and Hegemann 2008) for three different cases. First, the particle was not considered and only the deformation of the cupula under the influence of the fluid flow was analyzed. Figure 4 shows the comparison of results of numerical simulation with analytical solution published in the literature (Obrist and Hegemann 2008). As it can be seen, the cupular displacement during the head movement changes proportionally to the angular velocity. After the head rotation has finished, at time point $t = 0$ s, the cupula has an overshoot and exceeds the relaxed position in the opposite direction and then slowly returns to the relaxed position over time. The results of numerical simulation agree well with analytical solution.

Then, the effect of the particle was introduced. First, the radius of the particle was taken to be 20 μm. Figure 5 shows the change of cupular displacement over time, obtained in numerical simulations, in comparison with results from the literature. Figure 6 shows similar results, but for a particle with smaller radius of 15 μm. In the presented model, a single particle is considered, but all quantities relevant for the simulation (mass, particle radius, Stokes force coefficient, gravity force, etc.) are multiplied with the number of particles that are considered. This way, the effect of various particles is actually simulated. This is similar to the approach proposed by Obrist, but not the same, due to the differences in the mathematical model, i.e., in the equations for the motion of the particle. During the head movement, the cupular displacement obtained in numerical simulation agrees well with

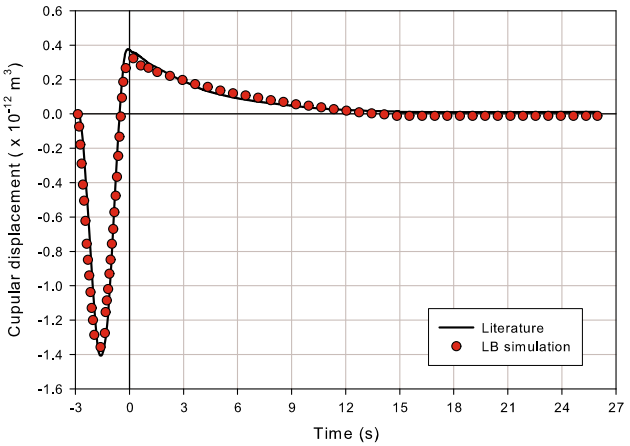

Fig. 4 Change of cupular displacement over time, when the effect of the immersed particle is neglected; *red dots* represent results obtained using numerical simulations, *solid line* represents results from the literature (Obrist and Hegemann 2008)

analytical results, because the endolymph flow has the major influence on the displacement. After the head rotation has finished, only the particle is causing the flow and the deformation of the cupula. These differences in the model for the motion of the particle cause the small disagreement of numerical and analytical results in Fig. 6 and this will be discussed in detail in the sequel.

The change of axial particle velocity during the simulation was also compared with results from the literature (Obrist and Hegemann 2008). The one-dimensional and two-dimensional particle models presented in the literature were compared with the proposed numerical model that simulates a full three-dimensional motion of the particle. Figure 7 shows the comparison of obtained results for a particle with radius of 15 μm. Figure 8 shows the comparison of results for a particle with radius of 25 μm. The axial velocity of the particle is a relative velocity, measured with respect to the wall of the domain and that is why the value of the velocity on the graphs is negative. Although the results are not identical for the three different models, similar results demonstrate that all methods show the same behavior of the observed quan-

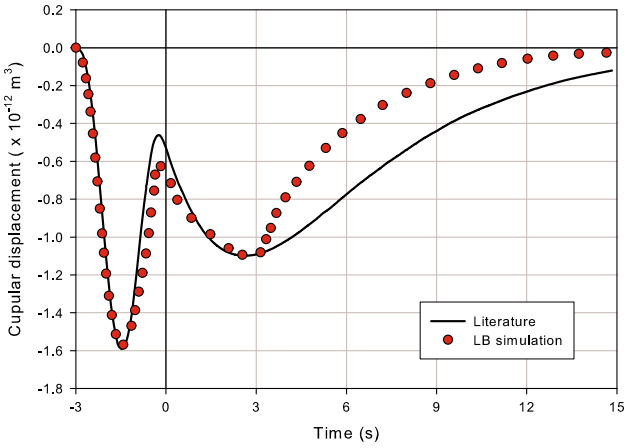

Fig. 5 Change of cupular displacement over time, when the effect of the immersed particle with radius of 20 μm is introduced; *red dots* represent results obtained using numerical simulations, *solid line* represents results from the literature (Obrist and Hegemann 2008), using the one-dimensional model

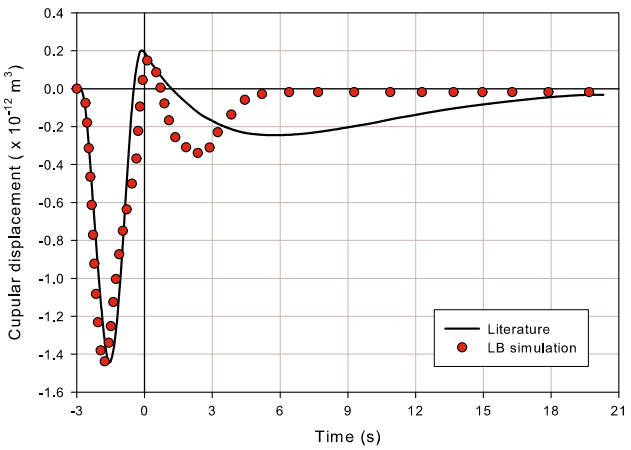

Fig. 6 Change of cupular displacement over time, when the effect of the immersed particle with radius of 15 μm is introduced; *red dots* represent results obtained using numerical simulations, *solid line* represents results from literature (Obrist and Hegemann 2008), using the one-dimensional model

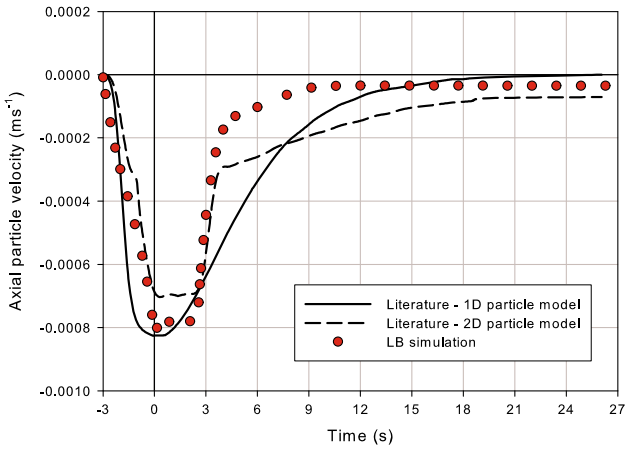

Fig. 7 Change of axial particle velocity over time, when the effect of the immersed particle with radius of 15 μm is introduced; *red dots* represent results obtained using numerical simulations, *solid line* represents results from the literature (Obrist and Hegemann 2008) for a one-dimensional particle model, and *dashed line* represents results from the literature (Obrist and Hegemann 2008) for a two-dimensional particle model

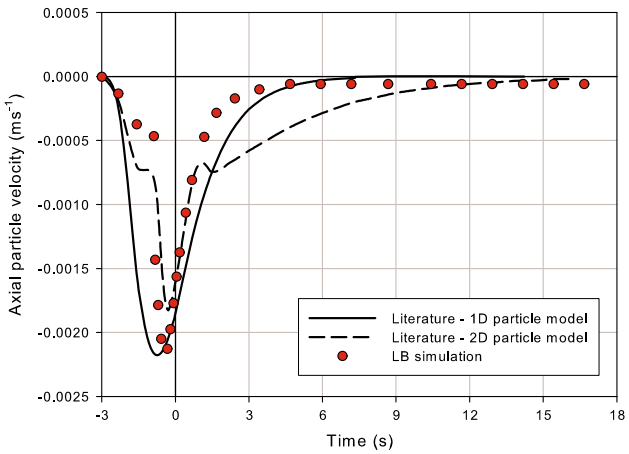

Fig. 8 Change of axial particle velocity over time, when the effect of the immersed particle with radius of 25 μm is introduced; *red dots* represent results obtained using numerical simulations, *solid line* represents results from literature (Obrist and Hegemann 2008) for a one-dimensional particle model, and*dashed line* represents results from the literature (Obrist and Hegemann 2008) for a two-dimensional particle model

tity. The trajectory of the particle in the observed plane (this plane is shown in Fig. 2) is also compared. Results obtained using the proposed numerical model and results from the literature are illustrated in Fig. 9. This comparison also shows that the similar behavior of the particle is obtained. It should be noted that in the proposed model a fully three-dimensional motion of the particle is analyzed. However, since there is no significant motion of the particle in the direction normal to the observed plane, this motion does not have a mayor influence on the overall solution. As it was explained in Sect. 2.4, when the distance between the particle and the wall becomes smaller than the lubrication gap, a repulsive force is included. In this case, when the particle is sliding along the wall, the influence of this repulsive force on the axial velocity of the particle becomes bigger and this causes the discrepancies between the results. Another fact that should be noted is that the repulsive force is acting along the normal to the wall in the specific point of the domain. In these simulations, a lubrication force that acts along the tangent to the wall is neglected. This could be another reason for the discrepancies between the results. In future improvements of the model, a more accurate way to simulate the interaction between the particle and the wall will be additionally considered.

The variation of simulation parameters was also considered within this study. The varied parameters are endolymph

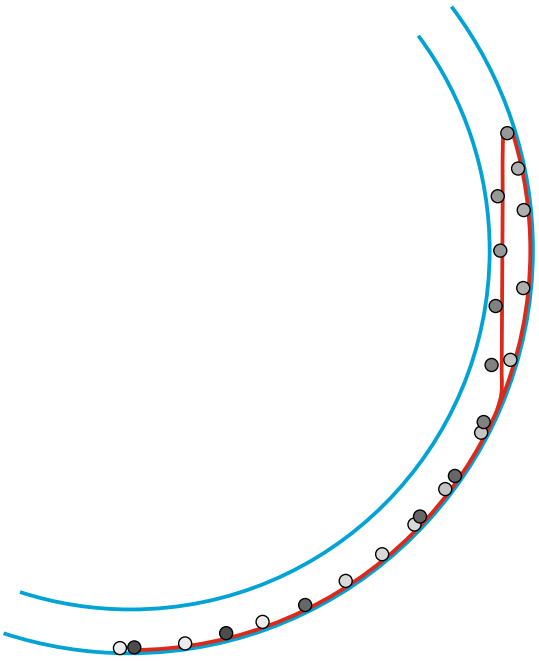

Fig. 9 Trajectory of the particle through the domain, when the radius of immersed particle is equal to 15 μm; *red solid line* represents results from the literature (Obrist and Hegemann 2008), *dots* represent results obtained using numerical simulations, whereas the *color* of the particle is darker as the time from the beginning of the simulation increases

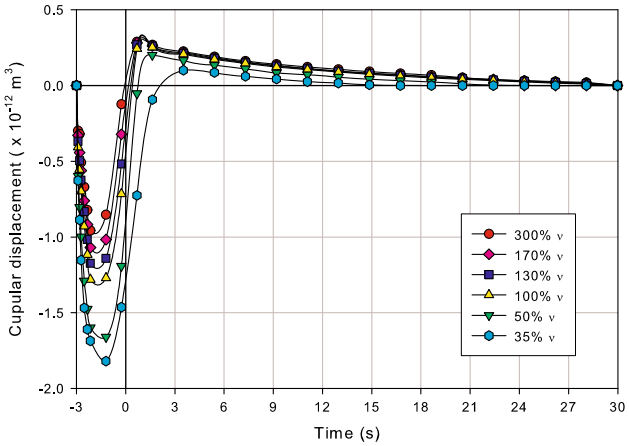

Fig. 10 Change of cupular displacement over time, for different values of endolymph viscosity, when the effect of the immersed particle is neglected

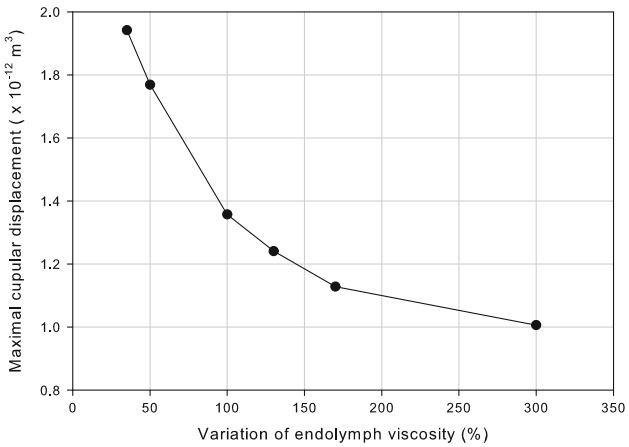

Fig. 11 Effect of variation of endolymph viscosity on the maximal cupular displacement, when the effect of the immersed particle is neglected

viscosity, cupular stiffness and lubrication gap. The parameters are varied from the initial values of these parameters that are given in Table 1. In this study, the wider range of particle sizes was not additionally considered, because the effect of this variation was already analyzed in the literature (Obrist and Hegemann 2008), so it is omitted here and only three particle sizes were used, in order to validate the results of numerical simulations.

First, the simulations were performed for the case when the effect of the particle was neglected. Figure 10 shows how the change of endolymph viscosity affects the change of cupular displacement over time. The value of endolymph viscosity has been established in the literature (Steer 1967), and the value used in this study is set accordingly. In the literature, it was also established that endolymph viscosity may be expected to vary due to the change in temperature at which it is measured (Gualtierotti 1981). In this study, the variation of this parameter was considered in numerical simulations to show to what extent does the viscosity of the endolymph influence the cupular displacement and to substantiate the previous conclusion that the disagreement obtained in Fig. 6 is due to the particle motion and not due to endolymph flow. It can be observed from Fig. 10 that if the viscosity is lower, there is a lower overshoot of the displacement, but also the reaction of the cupula to the surrounding fluid is slower. This can be explained by the fact that viscous forces in the fluid are smaller and thus this phenomenon occurs. The deformation of the cupula after the head rotation has finished is not significantly different for various values of endolymph viscosity, so it is obvious that here the change of endolymph viscosity has lower influence.

The sensitivity analysis, i.e., the effect of variation of endolymph viscosity on the maximum cupular displacement is shown in Fig. 11. Similar sensitivity analysis is shown in Fig. 12, but now the cupular stiffness is varied. As expected, from this graph it can be observed that when the cupula is stiffer, then the maximum displacement is smaller and vice versa.

Similar variations were performed in numerical simulations when a particle with radius of 20 μm was moving through the canal. Figure 13 shows the change of cupular displacement over time, when cupular stiffness was varied. With increase in cupular stiffness, the displacement decreases

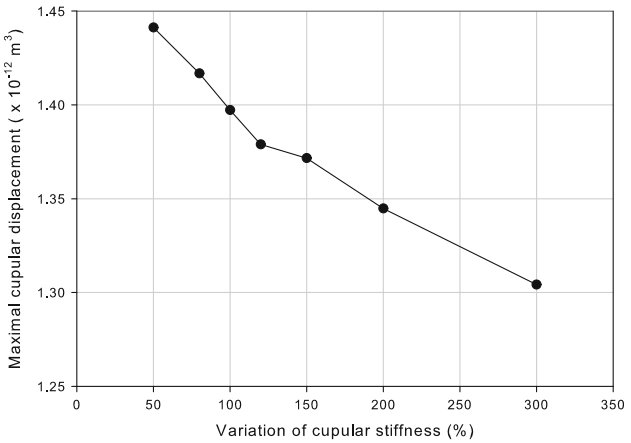

Fig. 12 Effect of variation of cupular stiffness on the maximal cupular displacement, when the effect of the immersed particle is neglected

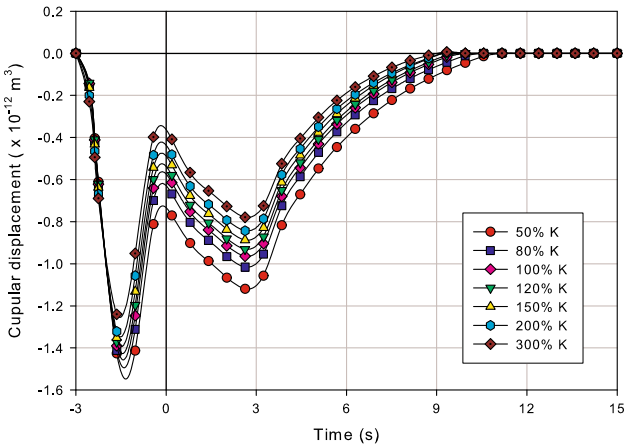

Fig. 13 Change of cupular displacement over time, for different values of cupular stiffness, when the effect of the immersed particle with radius of 20 μm is introduced

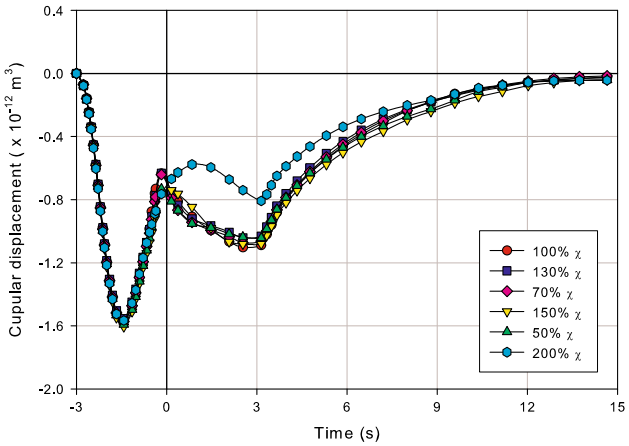

Fig. 14 Change of cupular displacement over time, for different values of lubrication gap, when the effect of the immersed particle with radius of 20 μm is introduced

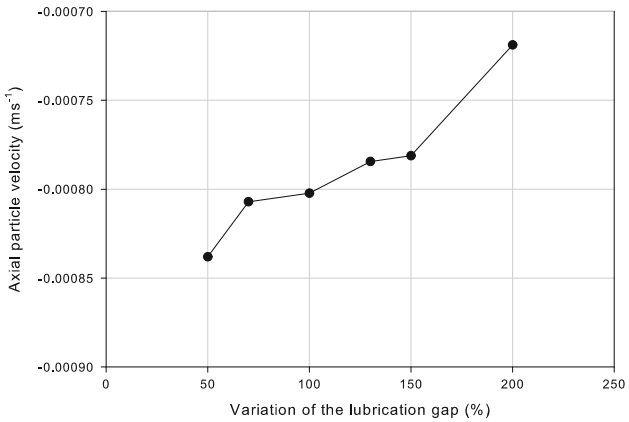

Fig. 15 Effect of variation of lubrication gap on the maximal axial particle velocity, when the effect of the immersed particle with radius of 15 μm is introduced

and vice versa, but the shape of the curve does not change significantly.

The lubrication gap that was imposed between the particle and the wall of the SCC was also varied, to analyze how this change affects the change of cupular displacement and the axial particle velocity. Figure 14 shows the change of cupular displacement over time, when a particle with radius of 20 μm is immersed in the canal, when the lubrication gap is varied. As it can be observed, a larger lubrication gap (2 times greater value) causes a significant variation in the shape of the curve representing the cupular displacement over time, like it is expected, because the particle is then closer to the centerline of the canal. Figure 15 shows the effect of the change of lubrication gap on the maximal axial particle velocity, when a particle with radius of 15 μm is immersed in the canal. The motion of the particle during the head maneuver is affected by the motion of the entire domain and the maximal axial particle velocity is affected by the force exerted from the fluid. If the particle is closer to the centerline of the canal, due to a larger lubrication gap, then the effect of the fluid is greater and the axial velocity has a higher value and vice versa.

5 Discussion and conclusion

Numerical simulations are used to model different phenomena. For example, behavior of red blood cells was extensively analyzed, as it is reviewed in literature (Fedosov et al. 2014), brain function was modeled using many diverse mechanical approaches, like it is reviewed in literature (Goriely et al. 2015). Blood flow and circulation in human body have also been extensively modeled in the literature, e.g., transport of LDL in arteries (Filipovic et al. 2014), blood and interstitial flow in the liver (Siggers et al. 2014), blood flow in arteries

that was coupled with a bioheat model of the surrounding tissue (Coccarelli et al. 2015).

The analysis of endolymph flow within the SCC and the BPPV syndrome has also already been studied in the literature. Van Buskirk et al. (1976) used Navier–Stokes equations to model the endolymph flow. Damiano and Rabbitt (1996) used an asymptotic form of the Navier–Stokes equations to estimate the velocity field in a three-dimensional SCC and the cupular displacement. Boselli et al. (2013b) modeled the endolymph flow in the whole SCC and focused on the flow in the utricle and in the ampulla. Same authors proposed a new numerical method that was applied to model the process of canalithiasis (Boselli et al. 2013a). They coupled the method of fundamental solutions with the force coupling method and modeled the endolymph flow using a mesh-free method, assuming that it can be modeled using the quasi-steady Stokes equations. Also, the flow field close to the solid particle was computed numerically, while the flow far from the particle was approximated by a Poiseuille flow. This numerical model was further used in the literature (Boselli et al. 2014) to analyze the motion of particles and cupular displacement when the head maneuvers are repeated causing the change of trajectories of the particles. Ifediba et al. (2007) used the exact geometry extracted from a specific patient, to predict the cupular displacement and they focused on analyzing the effect of geometrical parameters on the information forwarded to the brain from the vestibular system. Similarly, the finite element method was used in the literature (Sun et al. 2002) to model the human middle ear, using the geometry extracted from clinical data. Obrist (2008) analyzed a single SCC and defined the relationship between cupular displacement and head movement. This analysis was further expanded in the literature (Obrist and Hegemann 2008), and the findings of that paper were used in this study, to compare the results of numerical simulations. Squires et al. (2004) developed a two-dimensional model and quantified the effect of free-moving otoconia particles to the cupular displacement and nystagmus. Rajguru et al. (2005) used real geometry of the human membranous labyrinth and performed three-dimensional simulations. The system of ODE equations was solved using a fifth-order Runga–Kutta–Fuehlberg method, and the endolymph was assumed to undergo the Poiseuille flow.

This study presents a three-dimensional numerical model that is capable of simulating a complete three-dimensional motion of particles within the lumen of the SCC, where the endolymph is also moving freely, and the flow of endolymph is affected by the motion of both the whole domain and the immersed particles. In the study, an idealized geometry of the SCC was used, where the SCC was assumed to be circular, with a circular cross section. This simplification was introduced in order to be consistent with the similar idealization that was introduced in the literature (Obrist and Hegemann 2008). It should be noted that the authors in the cited literature used an additional inertial force to simulate the effect of the utricle and their geometry included only the narrow part of the SCC. On the other hand, in the proposed model, it is assumed that the entire domain has a circular cross section. The reason for this simplification was to perform simulations with a higher resolution of the domain, avoiding the details and focusing on the motion of the particle. The comparison of results showed that the presented numerical model can be used to predict the cupular displacement as a response to the particle motion. After this initial study where the main goal was to investigate the capabilities of the proposed model, the numerical model will be further expanded to enable simulations with geometries obtained from real clinical data, where the shape of the SCC and the cross section of the SCC would not be circular, but have the exact shape present in humans, to ensure highly accurate geometrical conditions. In the presented model, the cupula was assumed to be linearly elastic. In future improvements of the numerical model, more complex models of the cupula that were experimentally defined in the literature (Yamauchi et al. 2001) will be incorporated. Another simplification of the proposed model is the fact that the interaction between the immersed particle and the wall is modeled only along the normal to the wall of the SCC, while the tangent component is neglected. This simplification is the cause for the discrepancies that appeared during the comparison of results presented in Sect. 4. In future improvements of the model, a more detailed model of the interaction between the particle and the wall will also be incorporated.

The actual size, shape and number of particles in the SCC during canalithiasis is not known, and it can hardly be experimentally analyzed. In this case, numerical simulations can be helpful. Numerical simulations can be performed on a wide range of sizes of particles, in order to determine the most probable size that caused clinically observed symptoms.

Treatment of patients with balance disorders is a complex and difficult process, because it should be based on a complete diagnosis and it should be defined according to the specific symptoms and impairments that a patient is experiencing. Thus, there is a need for development of a customized (personalized) model simulation. This biomechanical model should be able to predict the response of the vestibular system of the patient to external perturbations under various pathological conditions. This can help early diagnostics, treatment planning and tracking of the progress of the balance disorder. The accuracy that was demonstrated in this study showed that the numerical model presented in this paper is a step toward this goal.

Acknowledgements This study was funded by grants from Ministry of Education, Science and Technological Development of the Republic

of Serbia (Projects Numbers III41007 and ON174028) and by FP7 ICT-2013-10 EMBalance Project.

Compliance with ethical standards

Conflict of interest The authors declare that they have no conflict of interest.

References

Baloh RW, Sloane PD, Honrubia V (1989) Quantitative vestibular function testing in elderly patients with dizziness. Ear Nose Throat J 68:935–939

Boselli F, Obrist D, Kleiser L (2013a) A meshless boundary method for Stokes flows with particles: application to canalithiasis. Int J Numer Methods Biomed Eng 29:1176–1191

Boselli F, Obrist D, Kleiser L (2013b) Vortical flow in the utricle and the ampulla: a computational study on the fluid dynamics of the vestibular system. Biomech Model Mechanobiol 12(2):335–348

Boselli F, Kleiser L, Bockisch CJ, Hegemann SCA, Obrist D (2014) Quantitative analysis of benign paroxysmal positional vertigo fatigue under canalithiasis conditions. J Biomech 47:1853–1860

Brandt T, Steddin S (1993) Current view of the mechanism of benign paroxysmal positioning vertigo: cupulolithiasis or canalolithiasis? J Vestib Res 3:373–382

Coccarelli A, Boileau E, Parthimos D, Nithiarasu P (2015) An advanced computational bioheat transfer model for a human body with an embedded systemic circulation. Biomech Model Mechanobiol. doi:10.1007/s10237-015-0751-4

Damiano E, Rabbitt R (1996) A singular perturbation model of fluid dynamics in the vestibular semicircular canal and ampulla. J Fluid Mech 307:333–372

Dix M, Hallpike C (1952) The pathology, symptomatology, and diagnosis of certain common disorders of the vestibular system. Proc R Soc Med 45:341–354

Djukic T, Topalovic M, Filipovic N (2015) Numerical simulation of isolation of cancer cells in a microfluidic chip. J Micromech Microeng 25(8):084012

Djukic T (2015) Modeling motion of deformable body inside fluid and its application in biomedical engineering. Dissertation, University of Kragujevac, Serbia

Dupin M, Halliday I, Care C, Alboul L, Munn L (2007) Modeling the flow of dence suspensions of deformable particles in three dimensions. Phys Rev E Stat Nonlin Soft Matter Phys 6(75):066707

Fedosov DA, Noguchi H, Gompper G (2014) Multiscale modeling of blood flow: from single cells to blood rheology. Biomech Model Mechanobiol 13(2):239–258

Filipovic N, Zivic M, Obradovic M, Djukic T, Markovic Z, Rosic M (2014) Numerical and experimental LDL transport through arterial wall. Microfluid Nanofluid 16(3):455–464

Filipovic N, Isailovic V, Djukic T, Ferrari M, Kojic M (2012) Multiscale modeling of circular and elliptical particles in laminar shear flow. IEEE Trans Biomed Eng 59(1):50–53

Goriely A, Geers MGD, Holzapfel GA, Jayamohan J, Jrusalem A, Sivaloganathan S, Squier W, van Dommelen JAW, Waters S, Kuhl E (2015) Mechanics of the brain: perspectives, challenges, and opportunities. Biomech Model Mechanobiol 14(5):931–965

Hall SF, Ruby RR, McClure JA (1979) The mechanics of benign paroxysmal vertigo. J Otolaryngol 8:151–158

House MG, Honrubia V (2003) Theoretical models for the mechanisms of benign paroxysmal positional vertigo. Audiol Neurootol 8:91–99

Huang K (1987) Statistical mechanics. Wiley, New York

Ifediba MA, Rajguru SM, Hullar TE, Rabbitt RD (2007) The role of 3-canal biomechanics in angular motion transduction by the human vestibular labyrinth. Ann Biomed Eng 35:1247–1263

Inagaki T, Suzuki M, Otsuka K, Kitajima N, Furuya M, Ogawa Y, Takenouchi T (2006) Model experiments of BPPV using isolated utricle and posterior semicircular canal. Auris Nasus Larynx 33:129–134

Krafczyka M, Cerrolazaa M, Schulza M, Ranka E (1998) Analysis of 3D transient blood flow passing through an artificial aortic valve by Lattice Boltzmann methods. J Biomech 31(5):453–462

Malaspinas OP (2009) Lattice Boltzmann method for the simulation of viscoelastic fluid flows. Dissertation, cole Polytechnique Fdrale de Lausanne, Switzerland

Min P (2013). Binvox 3D mesh voxelizer. http://www.patrickmin.com/binvox/. Accessed 01 July 2016

Nooruddin FS, Turk G (2003) Simplification and repair of polygonal models using volumetric techniques. IEEE Trans Vis Comput Graphics 9(2):191–205

Obrist D (2008) Fluid mechanics of semicircular canalsrevisited. Z Angew Math Phys 59:475–497

Obrist D, Hegemann S (2008) Fluidparticle dynamics in canalithiasis. J R Soc Interface 5:1215–1229

Parnes LS, McClure JA (1992) Free-floating endolymph particles: a new operative finding during posterior semicircular canal occlusion. Laryngoscope 102:988–992

Peskin CS (1977) Numerical analysis of blood flow in the heart. J Comput Phys 25(3):220–252

Rajguru SM, Rabbitt RD (2007) Afferent responses during experimentally induced semicircular canalithiasis. J Neurophysiol 97:2355–2363

Rajguru SM, Ifediba MA, Rabbitt RD (2005) Biomechanics of horizontal canal benign paroxysmal positional vertigo. J Vestib Res 15:203214

Schuknecht HF (1962) Positional vertigo: clinical and experimental observations. Trans Am Acad Ophthalmol Otol 66:319–331

Siggers JH, Leungchavaphongse K, Ho CH, Repetto R (2014) Mathematical model of blood and interstitial flow and lymph production in the liver. Biomech Model Mechanobiol 13(2):363–378

Squires TM, Weidmann MS, Hain TC, Stone HA (2004) A mathematical model for top-shelf vertigo: the role of sedimenting otoconia in BPPV. J Biomech 37:1137–1146

Sun Q, Gan RZ, Chang K-H, Dormer KJ (2002) Computer-integrated finite element modeling of human middle ear. Biomech Model Mechanobiol 1(2):109–122

Sun C, Munn LL (2008) Lattice Boltzmann simulation of blood flow in digitized vessel networks. Comput Math Appl 55(7):1594–1600

Suzuki M, Kadir A, Hayashi N, Takamoto M (1996) Functional model of benign paroxysmal positional vertigo using an isolated frog semicircular canal. J Vestib Res 6:121–125

Van Buskirk W, Watts R, Liu Y (1976) The fluid mechanics of the semicircular canals. J Fluid Mech 78:87–98

Wu J, Shu C (2010) Particulate flow simulation via a boundary condition-enforced immersed boundary-lattice Boltzmann scheme. Commun Comput Phys 7(4):793–812

Yamauchi A, Rabbitt R, Boyle R, Highstein S (2001) Relationship between inner-ear fluid pressure and semicircular canal afferent nerve discharge. J Assoc Res Otolaryngol 3:24–44

Yu H, Chen X, Wang Z, Deep D, Lima E, Zhao Y, Teague SD (2014) Mass-conserved volumetric lattice Boltzmann method for complex flows with willfully moving boundaries. Phys Rev E 89:063304